Biochemistry

pubs.acs.org/biochemistry Article

Insights into Binding of Single-Stranded Viral RNA Template to the Replication–Transcription Complex of SARS-CoV-2 for the Priming Reaction from Molecular Dynamics Simulations

Jimin Wang,* Yuanjun Shi, Krystle Reiss, Brandon Allen, Federica Maschietto, Elias Lolis, William H. Konigsberg, George P. Lisi, and Victor S. Batista*

Cite This: https://doi.org/10.1021/acs.biochem.1c00755 Read Online

ACCESS | Metrics & More | Article Recommendations | Supporting Information

ABSTRACT: A minimal replication–transcription complex (RTC) of SARS-CoV-2 for synthesis of viral RNAs includes the nsp12 RNA-dependent RNA polymerase and two nsp8 RNA primase subunits for *de novo* primer synthesis, one nsp8 in complex with its accessory nsp7 subunit and the other without it. The RTC is responsible for faithfully copying the entire (+) sense viral genome from its first 5′-end to the last 3′-end nucleotides through a replication-intermediate (RI) template. The single-stranded (ss) RNA template for the RI is its 33-nucleotide 3′-poly(A) tail adjacent to a well-characterized secondary structure. The ssRNA template for viral transcription is a 5′-UUUAU-3′ next to stem-loop (SL) 1′. We analyze the electrostatic potential distribution of the nsp8 subunit within the RTC around the template strand of the primer/template (P/T) RNA duplex in recently published cryo-EM structures to address the priming reaction using the viral poly(A) template. We carried out molecular dynamics (MD) simulations with a P/T RNA duplex, the viral poly(A) template, or a generic ssRNA template. We find evidence that the viral poly(A) template binds similarly to the template strand of the P/T RNA duplex within the RTC, mainly through electrostatic interactions, providing new insights into the priming reaction by the nsp8 subunit within the RTC, which differs significantly from the existing proposal of the nsp7/nsp8 oligomer formed outside the RTC. High-order oligomerization of nsp8 and nsp7 for SARS-CoV observed outside the RTC of SARS-CoV-2 is not found in the RTC and not likely to be relevant to the priming reaction.

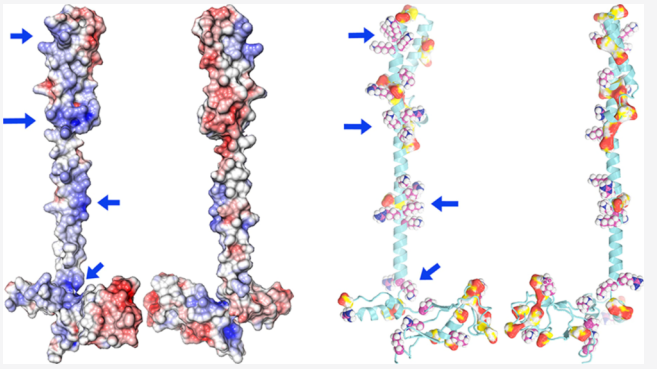

INTRODUCTION

Primase synthesizes short RNA primers both for DNA polymerases (pols), which cannot synthesize a primer *de novo*, and for some RNA pols that are incapable of synthesizing primers, including the RNA-dependent RNA polymerase (RdRp) nsp12 of SARS-CoV-2.[1−3] Therefore, primase is an essential component of the replication and transcription complexes (RTC). Many RNA pols are bifunctional and can carry out both primer synthesis and primer elongation, such as the single-subunit T7 RNA pol, the multi-subunit *E. coli* RNA pol, and the eukaryotic RNA pol II.[4−7] Primer synthesis and primer elongation, however, are two distinct processes. A phase transition from primer synthesis to primer elongation often involves dramatic unfolding-refolding-like conformational changes as if they were two completely different enzymes, folded from the same single polypeptide sequences.[8] During primer synthesis in transcription, RNA pols recognize the promoter sequence and bind it tightly.[4−6] The free energy of this binding enables the enzymes to melt and unwind the DNA duplex, forming a transcription bubble where *de novo* primer synthesis occurs. Before the transition from primer synthesis to primer elongation, RNA pols must undergo a significant conformational change to escape from the tightly bound promoter, a process known as promoter escape; otherwise, the pols will keep synthesizing short RNA primers in a process known as the abortive cycle of primer synthesis.[9] To avoid the complexity of the transition from primer synthesis to primer elongation, many viruses often encode their own primase with the exception of a few notable examples, such as HIV.[3,10,11] Instead, HIV packs in its mature virion at high concentration of human $tRNA^{Lys3}$, which serves as a primer for the first run of DNA synthesis. Then, the HIV reverse transcriptase retains a special poly-purine-track (PPT) sequence of its genome to serve as a primer for the second run of DNA synthesis.

Received: November 19, 2021
Revised: February 9, 2022

Many coronaviruses, including SARS-CoV, SARS-CoV-2, and murine hepatitis virus (MHV), encode a very small primase nsp8 and an accessory subunit nsp7.[3] How the primase binds and recognizes the preferred priming sequence from the templates of SARS-CoV-2 remains puzzling and is the subject of our study. The *de novo* primer synthesis by SARS-CoV-2 nsp8 primase involves the binding of the template strands plus two UTPs during the replication-intermediate (RI) synthesis or two ATPs during viral transcription, all of which have multiple negative charges.[3] For this feature, the primase activity is prone to inhibition by citrate and other multivalent anions as observed in the human primase.[12] Yet, the isoelectric point of the SARS-CoV nsp8 primase is 6.5, which shows clearly that it is an acidic protein that differs from many basic nucleic acid-binding proteins.[13] Therefore, the binding of both the templates (and template/primer) and two initiation NTPs requires special clustering of positively charged residues (Arg/Lys). When nsp8 and nsp7 of SARS-CoV were mixed in a one-to-one ratio, they formed a stable hexadecamer with a central pore where many positively charged residues are clustered.[13,14] The size of the pore is comparable to that of the replication processive factor sliding-clamp protein, leading to the hypothesis that this pore binds nucleic acids. The nsp8 primase can synthesize RNA primers with a moderate efficiency in the presence of nsp7 outside the RTC, but with reduced efficiency in its absence.[15,16] Site-directed mutagenesis of some positive residues (*i.e.*, K58A) greatly impaired the *de novo* primer synthesis, supporting the hypothesis that the oligomerization might be important for the priming reaction.[15,16]

There are several issues with the current hypothesis for the priming-active form of the nsp8 primase. The high-order oligomers of nsp7/nsp8 that were observed for SARS-CoV have not yet been observed for SARS-CoV-2. For SARS-CoV-2, there are two copies of the same nsp8/nsp7 complex present in the asymmetric unit in two crystal structures (*i.e.*, the molar ratio of nsp8 to nsp7 is one-to-one, but not two-to-one as observed in the RTC), but they do not form the same high-order oligomers as SARS-CoV.[17−20] Only a single nsp8/nsp7 heterodimeric complex was found inside the nsp8/nsp7/nsp12 RTC of SARS-CoV-2, with no evidence of any other high-order oligomers.[21] The second nsp8 subunit within the RTC does not interact with an accessory subunit. If the hypothetical nsp7/nsp8 oligomers are indeed required for the priming reactions, many other intermediates should exist,[22] none of which have been observed. These oligomers would have to be extensively remodeled so that the *de novo* synthesized primer inside the central pore could be transferred and loaded onto the RTC for primer elongation.[22] Moreover, the catalytically important carboxylates D50/D52 of the nsp8 primase are partially buried at the oligomeric interface.[16] Many other cryo-EM structures of the nsp8/nsp7/nsp12 subcomplexes from SARS-CoV-2 have been reported.[21−33] These structures contain a variety of primer/template (P/T) RNA duplexes with the 3′-end of the primer strand at the pol active site (or near it), including the substrate complex, the product complex with or without the pyrophosphate product bound, the remdesivir (or other nucleotide analog)-containing complexes, the post and pre-translocation complexes, the backtracking complexes with different lengths of unpaired 3′ primers, a gapped P/T duplex complex, and a strand-displaced P/T duplex complexes. All contain a conserved nsp8/nsp7/nsp12/nsp8 core.

A typical RTC includes two helicase nsp13 subunits, which are responsible for unwinding the secondary structures of the RNA template stem and pseudoknot structures and for strand-switching events. It is responsible for faithfully copying the entire (+) viral genome from the first 5′-end nucleotide to the last nucleotide of the 3′-poly(A) tail through a replication intermediate (RI) template.[34−36] There are 36 unstructured nucleotides at the 3′-tail exiting from the P5 stem of the SARS-CoV-2 genome, including a 33-nucleotide poly(A) tail. This template is faithfully copied into a 33 nucleotide 5′-poly(U) in the RI sequence. This sequence is unique only to the RNA virus known as the poly(U) negative-sense (PUN) template of transcription intermediate (TI) and often elicits a strong immune response.[37] Remarkably, the nsp13 helicase is not required to unwind the template for the priming reaction when the template is already single-stranded (ss).

Here, we focus on analysis of the viral ss-poly(A) template binding at the RTC and how it provides support to the mechanistic hypothesis that this binding would be competent for the priming reaction. In the RTC complex, D50/D52 of both primase subunits are exposed. We provide molecular dynamics (MD) simulations to show that an arrangement of positive residues on these nsp8 primase subunits within the RTC can bind ssRNA templates.

MATERIALS AND METHODS

The RNA-backtracked 7krp RTC structure (determined using cryo-electron microscopy at 3.2-Å resolution)[21] was selected as a starting point for our MD simulation (Figure 1). The RTC structure includes the RNA polymerase nsp12, one primase nsp8 subcomplex with its accessory subunit nsp7, another nsp8 without it, and a P/T double-stranded (ds) RNA duplex. Divalent metal ions and other ligands were removed from the structure and three runs of MD simulations were carried out with (i) a P/T duplex complex as it was in the 7krp structure; (ii) after removal of its primer strand; and (iii) after replacement of all 36-nucleotides in the template with a model of 36-nucleotide ss-poly(A), which was built using the Mutagenesis Wizard of Pymol.[38]

Schrödinger's Maestro was used to prepare the complex structure for MD simulations,[39] including Protein Preparation Wizards for assignment of bond orders and protonation states and for addition of missing H atoms and side chains. The complex was placed in a water box of 116 Å × 182 Å × 165 Å with a cushion of ∼15 Å from the complex boundary. Na^+ ions were added to neutralize the complex. The topology and parameters were generated using the LEaP program of the AmberTools package.[40] MD simulations were carried out using the program NAMD (nanoscale MD) after the following 3-step initial energy minimization,[41,42] including (i) 50 ps-position optimization of water molecules with the protein−nucleic acids structure fixed, (ii) 50 ps position side-chain optimization, and (iii) 100 ps global position optimization. Equilibrium was performed at 310 K, corresponding to the physiological temperature of the human body. MD simulations over 100 ns were carried out with an increment of 2 fs per step.

We analyzed initially 3750 frames from 75 ns MD trajectories and then all 5000 frames from 100 ns after removing all water molecules. All MD configurations were aligned and written out into individual PDB files, one file per trajectory, using VMD.[43] MD-derived electrostatic potential (ESP) maps were calculated using the CCP4 suite as follows.[44] Each aligned PDB file was moved to the center of a box of 120

https://doi.org/10.1021/acs.biochem.1c00755
Biochemistry XXXX, XXX, XXX−XXX

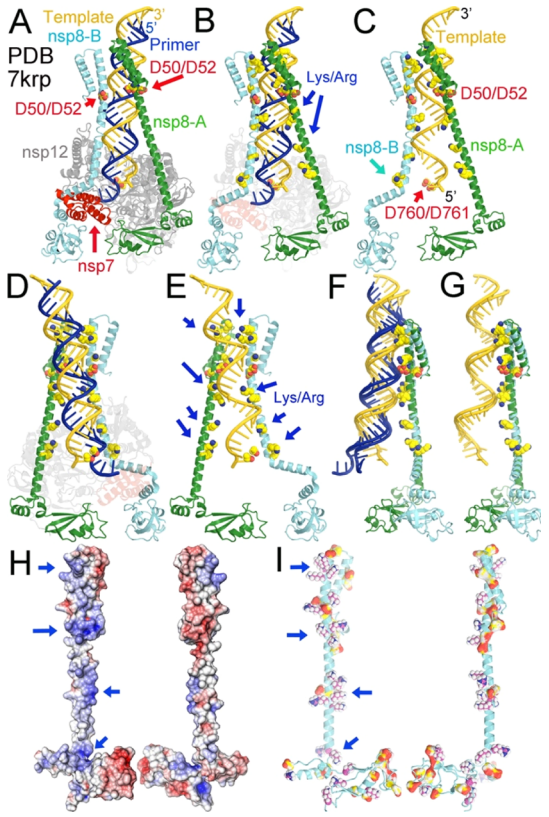

Figure 1. 7krp structure of the RTC and electrostatic properties of the nsp8 primase. (A) Overall structure: nsp12 RNA polymerase (gray), nsp7 (red)-bound nsp8 (cyan, nsp8-B), nsp7-free nsp8 (green, nsp8-A), primer (blue)/template (gold) RNA duplex with the primase active D50/D52 residues, and pol-active D760/761 residues in red spheres. (B) Positive Lys/Arg residues on both nsp18 subunits are shown in the CPK model. (C) Template strand-nsp8 interactions after the primer strand, nsp12, and nsp7 subunits are removed. (D,E) Rear views of (B,C). (F) Superposition of nsp8-A and nsp8-B with the P/T RNA duplex bound shows a conserved nsp8-RNA duplex interacting mode. (G) Template strand−nsp8 interactions after the primer strand is removed. (H) Two 180° views of the electrostatic model of nsp8. (I) Two views of CPK models of nsp8 with positive Lys/Arg residues. Arrows indicate four patches of positive Arg/Lys residues of nsp8 (the first to the fourth from top to bottom). Cluster Cα−Cα spacing of positively charged residues is 15.4 ± 2.0 Å.

Å × 180 Å × 160 Å using the routine pdbset of CCP4.[44] Structure factors were calculated using a library of electron scattering factors for neutral atoms with the program sfall at 1.0 Å resolution, at grids of 340 Å × 532 Å × 480 Å with an added ΔB-factor value of 8 Å^2 to minimize the Fourier series termination effect.[44] ESP maps were calculated using the routine fft, and the all ESP maps are averaged using the program mapsig.[44] For detailed calculations, an example command script file is provided in online Supporting Information along with self-explanatory instructions and self-contained dependent scripts.

The equilibrated model of the 7krp structure was fitted into the MD-ESP maps using the program Chimera and refined against them using both Phenix and Refmac5 of CCP4.[44−46] The model was rebuilt using the graphics program Coot in 3- to 6-passes of iterations refined using Refmac5.[45,47] Figures were made using the program Pymol.[38] Molecular ESP was calculated using the program PDBj/F-surf at pH 7.0 and 0.1 M NaCl.[48]

RESULTS AND DISCUSSION

Basic Features of nsp8 Primase within the Existing Structures of the RTC and within the nsp7/nsp8 Oligomers. Figure 1 shows the 7krp structure of the nsp8/nsp7/nsp12 P/T complex of SARS-COV-2, the charge-only ESP feature of the nsp8 primase, and the distribution of positive residues (Lys/Arg) on nsp8.[21] The primer strand has three unpaired nucleotides at the 3′-end and permits the P/T duplex to backtrack by three nucleotides away from the polymerase active site. Backtracking is a common mechanism that permits unpaired nucleotides of the primer stand to move into the nsp14 exoribonuclease active site for removal of mispairings. However, we find that a remdesivir monophosphate (RMP)-added primer strand remains Watson−Crick base-paired with the templating U base and does not backtrack readily, highlighting the robustness of the resulting complex.[26] The pol-catalytic carboxylates (D760/D761 of the nsp12) and primase carboxylates (D50/D52) of the nsp8 primase active site are separated by ∼60 Å or two helical turns of the RNA duplex.

The nsp7-free nsp8 subunit has an "L" shape and a golf club-like structure with a long helix N-terminal domain (αB) and a compact C-terminal domain (CTD) for binding to nsp7 (see below), linked by a short helix (αC) (Figure 2). The helical domain has a hairpin with another short helix (αA). The two known catalytic carboxylates D50/D52 responsible for the priming activity are located at the junction near the N-terminal domain (NTD) of the first helix αA.[15,16] The nsp7-bound nsp8 subunit has a kink in the long helix (αB + αB′), positioning four patches of positively charged Lys and Arg residues evenly spaced along the long helix αB although the number of charges in each patch varies. The spacing of positive residues matches nearly perfectly the pitch of P/T RNA duplex in A-form bound within the RTC such that these positive charges are responsible for high-affinity binding to the phosphate backbone of the P/T duplex. The structural model shows that the spacing should match the pitch of the B-form DNA duplex as well after slightly tilting the helical axis of the protein relative to the helical axis of the duplex. In fact, the nsp8 primase can efficiently use a ssDNA template to synthesize RNA primers *de novo*.[15]

A reorientation of αB of nsp8-A has been observed to rotate by about 45° away from its normal position in an RTC complex containing a strand-displaced P/T duplex (the fraction was so low that the coordinates of that structure were not provided by authors).[22] This new orientation likely aligns with the displaced RNA strand. In the absence of nucleic acid, in the apo nsp8/nsp7/nsp12 structure, both αA and αB helices of nsp8 are completely disordered. All these observations suggest that the αB helix of nsp8 provides a scaffold for binding both the ssRNA template and the dsP/T RNA duplex product of the priming reaction. Upon *de novo* synthesis of short RNA primers by nsp8, spiral translocation of the P/T move the synthesized primer into the pol active site for primer elongation (separated by ∼two helical turns or ∼60 Å). All current structures of the RTC complexes represent conformations after such a translocation step.

Catalytic carboxylates are responsible for the negative ESPs of the active site of DNA and RNA pols (including the RNA polymerase nsp12 of SARS-CoV-2) before the binding of two divalent metal ions. However, that distinct feature is not observed in the molecular ESP feature of the nsp8 primase

https://doi.org/10.1021/acs.biochem.1c00755
Biochemistry XXXX, XXX, XXX−XXX

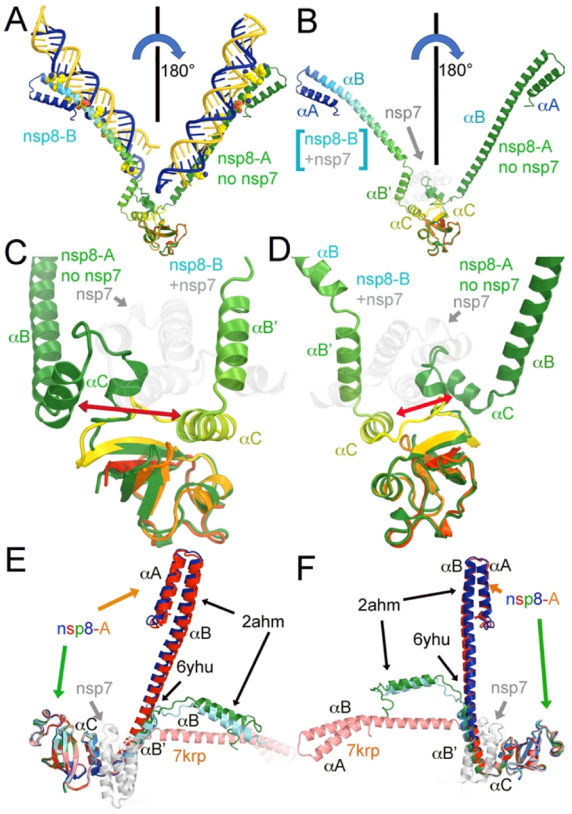

Figure 2. Conformations of nsp8. (A) Superposition of the CTD of the two nsp8 subunits within the RTC with bound P/T RNA duplex. (B) Removal of the P/T RNA duplex. (C,D) Two close-up views of the NTD/CTD junctions of the two nsp8 subunits. (E,F) Superposition of CTD of the nsp8 subunits (multicolor) with additional nsp7/nsp8 structures (2ahm, 6yhu, and 7krp) in complex with nsp7 (silver).

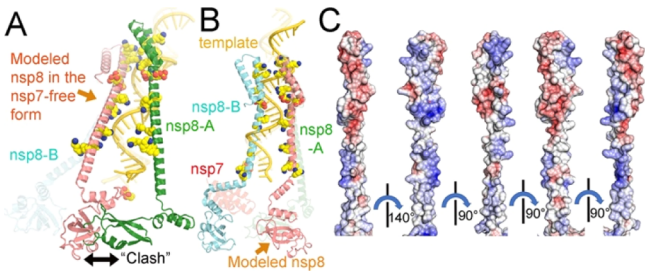

Figure 3. Conformation-dependent binding of nsp8 subunits to the ssRNA template. (A) Conformation of nsp8-A (salmon and green) in nsp8-B (light cyan) position. (B) Conformation of nsp8-B (salmon and cyan) in the nsp8-A (light green) position. (C) Close-up views of electrostatic potential of the nsp8 subunits in successive rotation of 140, 90, 90, and 90°.

subunit in the absence of divalent metal ions since nearby positive residues cancel the negative ESPs of these carboxylates (Figure 1H). It is also possible that local structural changes may occur when the primase binds the ssRNA template and that its structure may differ from the dsRNA bound form, particularly one lacking a free 3′-hydroxyl near the primase active site. Nonetheless, two carboxylates of both nsp8 subunits are very close to the primer strand of the P/T RNA duplex (Figure 1), suggesting that the overall conformation of the P/T RNA duplex may resemble that of the ssRNA template.

The interface between nsp7 and nsp8 is the only conserved structural feature among all nsp7/nsp8 complexes (such as 2ahm, 6yhu, 7krp, 7jlt, and 6wiq) (Figure 2),[13,17,19−21] which is present in all pol structures of SARS-CoV-2, as described previously.[21−33] Neither the hexadecameric nor the octameric nsp7/nsp8 complexes of SARS-CoV have been observed for SARS-CoV-2, either inside or outside the RTC. Therefore, the original hypothesis that the central pore of these oligomers binds the template for prime synthesis remains uncertain.[13,17,21] Moreover, the catalytic carboxylates (D50/D52) are partially buried at the oligomeric interface. These structural features combined with the results of our analysis suggest that the two nsp8 subunits within the RTC might be catalytically relevant, so the original mechanistic hypothesis that the RNA primer is synthesized inside the central pore of an isolated hexadecameric nsp7/nsp8 complex of SARS-COV might not be relevant to the priming reaction of the SARS-CoV-2 primase.[13] Likewise, it might no longer be necessary to assume that the hexadecameric complex would have to open to hand over the primer to the nsp12 polymerase of the RTC after synthesizing it inside the central pore.[22] Furthermore, we note that the positively charged αB of nsp8 is expected to bind to negatively charged surfaces of the adjacent nsp7/nsp8 complex, forming non-catalytic oligomers that may mislead the interpretation of experimental results.[13]

Binding of nsp7 to nsp8 rotates the helical domain of nsp8 by ∼180° around the axis that is ∼40° from the helical axis relative to the CTD of nsp8 (Figure 2). This rotation allows two nsp8 subunits to simultaneously bind to the same ssRNA template, one with nsp7-bound nsp8 while the other with nsp7-free nsp8. The rotation also allows two nsp8 subunits to bind to the nsp12 polymerase, simultaneously binding one P/T RNA duplex while positioning the 3′-hydroxyl of the primer strand at the pol-active site. Therefore, we analyzed whether the two nsp8 subunits in the same conformation of the nsp7-free (nsp8-A) or the nsp7-bound form (nsp8-B) could bind to the dsRNA or ssRNA in the same way as the two different conformations of the two nsp8 subunits observed in the RTC complex. Upon replacement of the nsp8-A form by the nsp8-B form, we find that the two nsp7-free nsp8 subunits cannot bind in the same way because their C-terminal domains would clash (Figure 3). However, when nsp8-B was replaced by nsp8-A, the two nsp7-bound nsp8 subunits could bind to the same dsRNA, or ssRNA, without clashing. Therefore, we consider that if the conformations of the two nsp8 subunits observed within the RTC are critical for the priming reaction, the two nsp8 subunits in the nsp8-B conformation could be catalytically active. Without nsp7, however, the ss-poly(A) template or P/T RNA duplex would not bind to two nsp8 subunits because the conformation of the nsp8 structure would be sterically hindered. In the presence of the nsp7 subunit, the conformation of the nsp8 primase becomes bent and rotates to a conformation that can bind to the nucleic acid substrate, providing a structural model for the enhanced efficiency of the nsp8 primase induced by nsp7.[15,16]

In addition to the four patches of positive electrostatic potential, there is a negative patch at the helical hairpin of nsp8 (Figure 3C) that can likely stabilize high-order oligomers by the hsp7/hsp8 heterodimeric complex. Positive and negative patches are distributed on the surface of the nsp8 subunit, oriented at about 140° apart (Figure 3C), so they can stabilize

https://doi.org/10.1021/acs.biochem.1c00755
Biochemistry XXXX, XXX, XXX−XXX

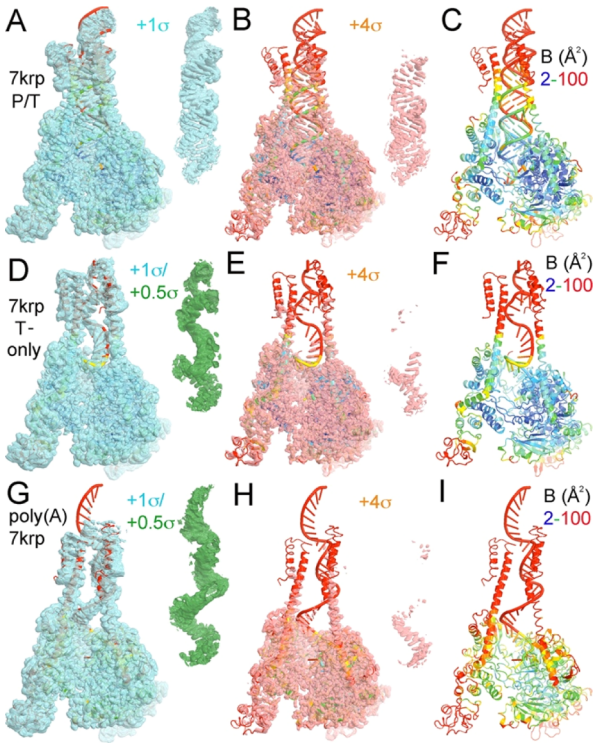

Figure 4. MD simulation-derived ESP maps for the 7krp complex with the bound P/T ds-RNA duplex (A−C), or the ssRNA template-only complex (D−F), or the modeled ss-poly(A) template complex (G−I). MD-ESP maps are contoured at low (+1σ, cyan; +0.5σ, green) and high (+4σ, salmon) contouring levels superimposed onto the corresponding atomic models, which are rainbow-colored by atomic B-factors, ramped up from 2 to 100 Å^2 (blue-to-cyan-to-red). Insets show ESP features for nucleic acids at low and high contouring levels.

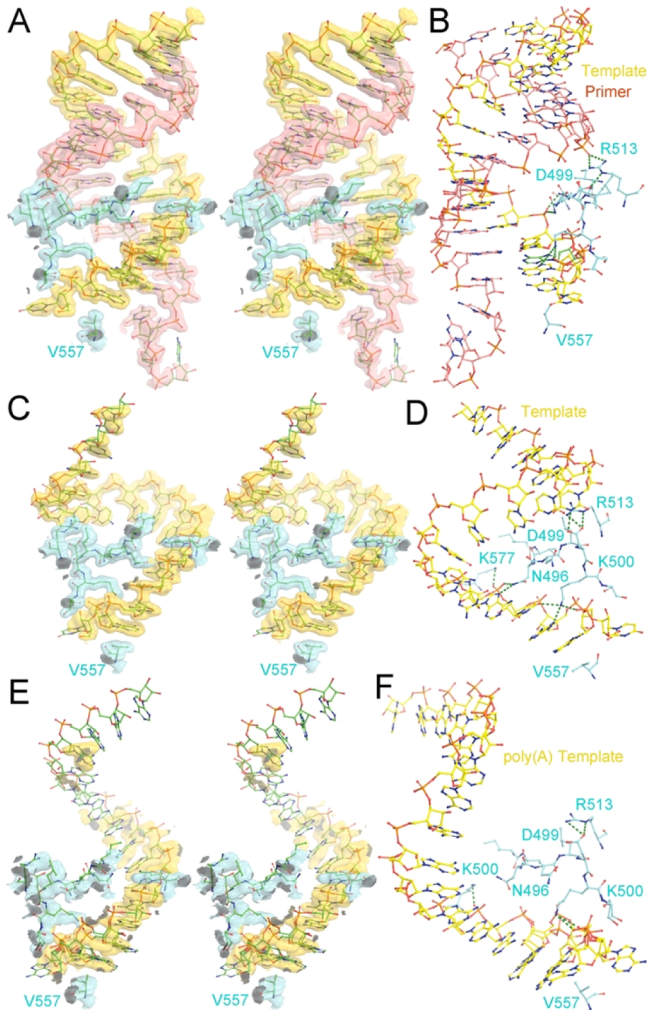

Figure 5. MD-ESP maps (contoured at +4σ) for the P/T dsRNA (A,B), for the template RNA-only (C,D), and for the poly(A) template (E,F) in the stereodiagram (A,C,E) and mono-view with detailed polymerase-nucleic acid H-bonds at the major groove of the P/T duplex (B,D,F). The pol nsp12 side chains and density are shown in cyan, templates in gold, and the primer in salmon. View orientations are the same for panels (A), (C), and (E), but different for panels (B), (D), and (F).

the two nsp8 subunits forming a concave surface where the ss-poly(A) template binds.

MD-Derived ESP Maps for the nsp8 Primase within the RTC. We hypothesize that the ssRNA template *alone* can bind to nsp8 by matching positive residues to the backbone phosphates of ssRNA as observed in the RTC. In that model, the ssRNA template can bind to two nsp8 subunits, so formation of the priming active complex requires one nsp8 subunit in the nsp7-free conformation and another one in the nsp7-bound conformation.

We carried out 100 ns MD simulations (Figure 4A−C) for the 7krp RTC complex containing (i) the original RNA sequence of the P/T duplex, (ii) after the removal of primer strand (Figure 4D−F), and (iii) after the replacement of 36-nucleotide template strand with a 36-nucleotide poly(A) template (Figure 4G−I) to test the hypothesis that patches of positive residues (Lys/Arg) provide a suitable ESP to anchor the ssRNA template for the priming reaction. Equilibrated models were derived and refined to 1.30 Å resolution with residual *R*-factors of 18.8, 25.0, and 23.2% between the MD-derived structure factors and model-derived structure factors for the three structures, respectively. The overall B-factors for these models are 48.0, 58.1, and 82.5 Å^2 (small uncorrected rotations of the entire molecule may account for an increased overall B-factor value). Corresponding root-mean-square derivations (rmsD) of the entire MD trajectories for all non-H atoms of the three MD structures are 0.78, 0.85, and 1.02 Å, respectively (rmsD = $[B/(8\pi^2)]^{1/2}$). They are equivalent to Wilson B-factors of crystallographic data sets, representing intrinsic dynamical properties that would limit the highest achievable local resolutions in the corresponding cryo-EM image reconstruction.

With a generic non-poly(A) template derived from the 7krp structure, the ssRNA template is rapidly refolded in MD trajectories to have a kink-like structure near the pol-active site (Figure 4D−F). The resulting configuration is distinct when compared to the helical conformation of dsRNA and positions the fourth patch of positive residues (Arg/Lys) of nsp8 near the pol-active site interacting with the phosphate backbone that is not present in the P/T duplex or the poly(A) template complex.

We find that the ss-poly(A) template remains largely in a helical conformation, as in the conformation of the P/T duplex (Figure 4G−I). Residues of both nsp8 subunits proximal to the catalytic residues (D50/D52) in the primase active site are more ordered than those that are far away from them, suggesting that the stable conformation of the stacked poly(A)

https://doi.org/10.1021/acs.biochem.1c00755
Biochemistry XXXX, XXX, XXX−XXX

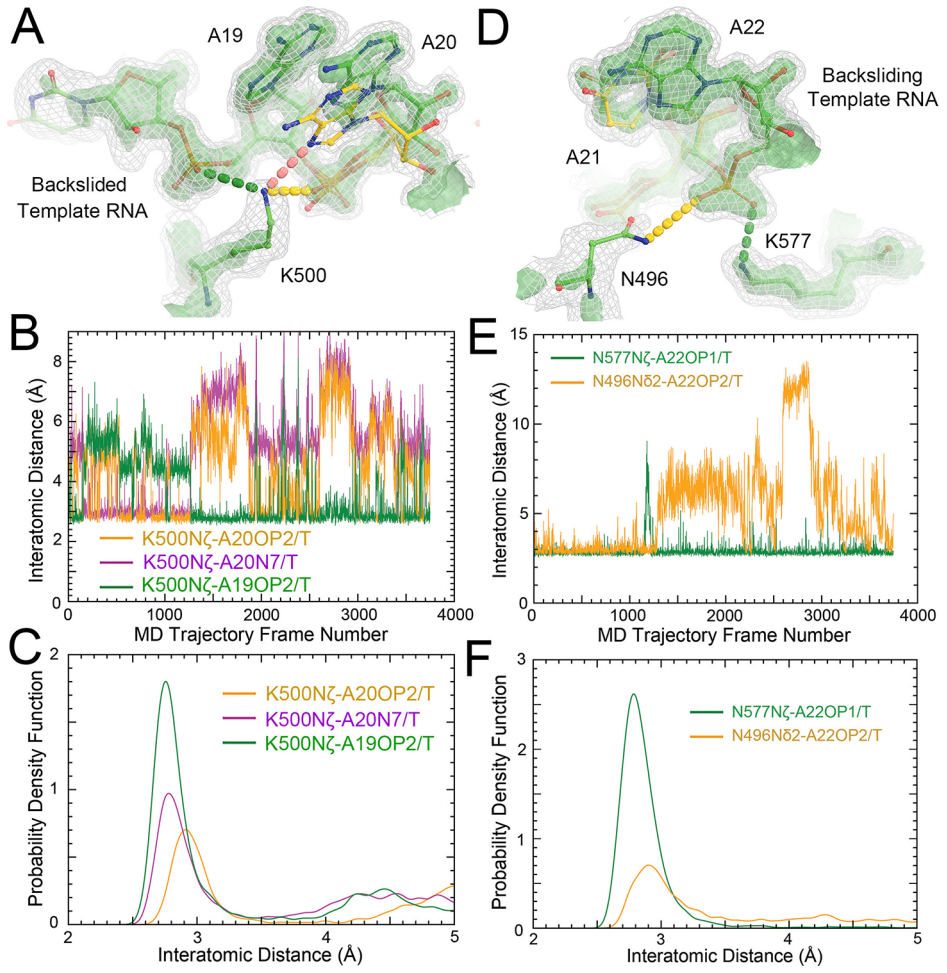

Figure 6. H-bonding patterns of backsliding and backslided complexes observed in MD simulations for the 7krp structure. (A−C). Three H-bonding patterns involving K500 of the polymerase are in three colors, with A19 phosphate (green), A20 phosphate (gold), and N7 of the A20 base in a minor conformation (salmon or magenta) of the RNA template strand. (A) MD-derived ESP maps contoured at high (+8σ, green isosurfaces) and low (+3σ, silver isomeshes) levels. (B) Interatomic distances as a function of the MD trajectory frame number. (C) Probability density function of interatomic distances. (D−F). Two H-bonding patterns involving K577 and N496 of the polymerase with the A22 phosphate.

structure bound to both the nsp8 primase subunits could be catalytically relevant. The stacked conformation in the poly(A) template is much stronger than a generic ssRNA template, which allows its phosphate backbone to deviate from the helical conformation through attractive interactions with the fourth patch of positive residues of nsp8 subunits near the pol-active site of the nsp12.[49,50] However, it remains to be established whether atomic motions of the ss-poly(A) template and the nsp8 subunits are affected by divalent metal ions (Mg^{2+}) and incoming NTPs at the primase active site.

The structural model of the RTC with the P/T duplex equilibrated by our MD simulations is essentially the same as the experimental 7krp model although with much more reliable information on H-bonds due to the improved resolution relative to the cryo-EM map (Figure 5A,B).[21] We find that a β-like strand consisting of nsp12 primase residues I494−S501 is inserted into the major groove of the P/T duplex. V557 is packed against the nucleobase of the templating nucleotide which is responsible for unpairing of the mismatched RNA duplex, during the backtracking movement, for passing the mismatches into the exoribonuclease active site for hydrolysis. We also note that K500 interacts with the phosphate backbone of the template strand and with N7 of an A nucleotide, causing the template strand to adopt two alternative conformations locally at this location. Furthermore, N496 forms an H bond with the phosphate backbone of the template strand. Adjacent to this β-like strand, K577 interacts with the template strand, which remains in all three structures, and R513 interacts with the phosphate backbone of the primer strand, which remains in the non-poly(A) template (Figures 5, 6).

The MD-derived ESP map from the entire trajectories of the 7krp structure represents the underlying equilibrated structure for the backsliding complex (Figure 6). In fact, MD trajectories contain at least two distinct components: (i) backslided complex and (ii) backsliding complex. In the backslided complex (of a major fraction), K500 interacts with A19/A20 phosphates of the RNA template strand. In the backsliding complex (of a minor fraction), K500 interacts with N7 of A20. These two complexes are mutually exclusive in the MD trajectories, that is, K500 can be part of either one complex, but not both simultaneously, suggesting that the movement of K500 helps to the movement of the RNA template strand (Figure 6B). It is likely that the backsliding process observed in MD simulations is in fact biologically relevant to the translocation process of the RNA duplex immediately after incorporation of each nucleotide monophosphate and essential for the priming reaction by the nsp8 primase within the RTC.

https://doi.org/10.1021/acs.biochem.1c00755
Biochemistry XXXX, XXX, XXX−XXX

An interesting observation from our MD simulations was that the non-poly(A) template strand was rapidly refolded to a new stable conformation when the primer strand was removed from the complex (Figure 5C,D). Part of the refolded template was displaced toward the new position (that was occupied by the primer strand in the dsRNA complex), making a specific H-bond between D499 and the N3 of a U nucleobase. The refolded template makes stronger H-bonds with N496 relative to the dsRNA duplex, with well-defined MD ESP features (Figure 6). The refolding processing was not observed in the poly(A) template, where its helical conformation is more rigid than the non-poly(A) template, and it extends to the primase active site for the priming reaction (Figure 5E,F).

The distributions of ESP maps and atomic B-factors provided by MD simulations of our structural models bear a striking similarity with those obtained from the cryo-EM maps. In both cases, also the interior of the model has smaller atomic B-factors (higher local resolution), while the periphery loops have larger B-factors. We note that our MD simulations and analysis of ESP distribution on the nsp8 primase subunits within the RTC suggests that the nsp8 can bind to the ssRNA template in a helical conformation, particularly, the viral poly(A) template. However, coronaviruses also encode the accessory subunit nsp9, which can also bind to ssRNA (as well as ssDNA).[51−54] So, it remains to be established whether nsp9 is involved in the *in vivo* priming reaction, for example, by loading or transferring ssRNA templates onto the RTC for the priming reaction. The possible functions of nsp9 after the post-priming reaction have been discussed, most noticeably in the mononucleotide phosphate transfer reactions and cap synthesis.[55−57]

In summary, our structural analysis of the nsp7/nsp8 subcomplex within the RTC shows that the nsp8 subunit has a distribution of positive residues (Lys/Arg) ideally suited to provide complementary binding interactions with the backbone phosphate groups of the viral ss-poly(A) template. Optimal binding requires one nsp8 subunit in the nsp7-bound conformation and a second nsp8 subunit in the nsp7-free conformation, enabling cooperative binding of the template for the priming reaction, as revealed by our MD simulations. The resulting insights are particularly valuable since they suggest that the conformation of the isolated nsp7/nsp8 subcomplex outside the RTC might not be catalytically relevant for the priming reaction since the catalytic carboxylates (D50/D52) would not be properly positioned.

■ ASSOCIATED CONTENT

Supporting Information

The Supporting Information is available free of charge at https://pubs.acs.org/doi/10.1021/acs.biochem.1c00755.

Self-explanatory sample Unix script for calculating ESP maps from aligned MD trajectories using CCP4 (PDF)

Unix /bin/csh script file (ZIP)

■ AUTHOR INFORMATION

Corresponding Authors

Jimin Wang − *Department of Molecular Biophysics and Biochemistry, Yale University, New Haven, Connecticut 06520-8114, United States;* orcid.org/0000-0002-4504-8038; Email: jimin.wang@yale.edu

Victor S. Batista − *Department of Chemistry, Yale University, New Haven, Connecticut 06511-8499, United States;* orcid.org/0000-0002-3262-1237; Email: victor.batista@yale.edu

Authors

Yuanjun Shi − *Department of Chemistry, Yale University, New Haven, Connecticut 06511-8499, United States*

Krystle Reiss − *Department of Chemistry, Yale University, New Haven, Connecticut 06511-8499, United States*

Brandon Allen − *Department of Chemistry, Yale University, New Haven, Connecticut 06511-8499, United States;* orcid.org/0000-0002-5512-1892

Federica Maschietto − *Department of Chemistry, Yale University, New Haven, Connecticut 06511-8499, United States;* orcid.org/0000-0002-5995-2765

Elias Lolis − *Department of Pharmacology, Yale University, New Haven, Connecticut 06520-8066, United States;* orcid.org/0000-0002-7902-7868

William H. Konigsberg − *Department of Molecular Biophysics and Biochemistry, Yale University, New Haven, Connecticut 06520-8114, United States*

George P. Lisi − *Department of Molecular and Cell Biology and Biochemistry, Brown University, Providence, Rhode Island 02912, United States;* orcid.org/0000-0001-8878-5655

Complete contact information is available at: https://pubs.acs.org/10.1021/acs.biochem.1c00755

Author Contributions

J.W. and V.S.B designed the experiments. Y.S. carried out MD simulations with assistance from K.R.; J.W. and Y.S. carried out analysis of MD trajectories and wrote the draft manuscript. All authors were involved in the interpretation of results and writing of the manuscript.

Funding

This work was supported by the NIH grant GM136815-02.

Notes

The authors declare no competing financial interest.

■ ABBREVIATIONS

RdRp	RNA-dependent RNA polymerase
SARS-CoV-2	severe acute respiratory syndrome coronavirus 2
P/T	primer/template
MD	molecular dynamics
MD-ESP	MD-derived electrostatic potential maps
ssRNA	single-stranded RNA
dsRNA	double-stranded RNA duplex
CTD	C-terminal domain
NTD	N-terminal domain

■ REFERENCES

(1) Frick, D. N.; Richardson, C. C. DNA primases. *Annu. Rev. Biochem.* **2001**, *70*, 39−80.

(2) Kuchta, R. D.; Stengel, G. Mechanism and evolution of DNA primases. *Biochim. Biophys. Acta* **2010**, *1804*, 1180−1189.

(3) Sola, I.; Almazán, F.; Zúñiga, S.; Enjuanes, L. Continuous and discontinuous RNA synthesis in coronaviruses. *Annu. Rev. Virol.* **2015**, *2*, 265−288.

(4) Steitz, T. A. The structural changes of T7 RNA polymerase from transcription initiation to elongation. *Curr. Opin. Struct. Biol.* **2009**, *19*, 683−690.

(5) Chen, J.; Chiu, C.; Gopalkrishnan, S.; Chen, A. Y.; Olinares, P. D. B.; Saecker, R. M.; Winkelman, J. T.; Maloney, M. F.; Chait, B. T.; Ross, W.; Gourse, R. L.; Campbell, E. A.; Darst, S. A. Stepwise

promoter melting by bacterial RNA polymerase. *Mol. Cell* **2020**, *78*, 275−288.
(6) Kornberg, R. D. The molecular basis of eucaryotic transcription. *Cell Death Differ.* **2007**, *14*, 1989−1997.
(7) Tang, G.-Q.; Roy, R.; Ha, T.; Patel, S. S. Transcription initiation in a single-subunit RNA polymerase proceeds through DNA scrunching and rotation of the N-terminal subdomains. *Mol. Cell* **2008**, *30*, 567−577.
(8) Yin, Y. W.; Steitz, T. A. Structural basis for the transition from initiation to elongation transcription in T7 RNA polymerase. *Science* **2002**, *298*, 1387−1395.
(9) Cheetham, G. M. T.; Jeruzalmi, D.; Steitz, T. A. Structural basis for initiation of transcription from an RNA polymerase-promoter complex. *Nature* **1999**, *399*, 80−83.
(10) Tang, H.; Kuhen, K. L.; Wong-Staal, F. Lentivirus replication and regulation. *Annu. Rev. Genet.* **1999**, *33*, 133−170.
(11) Gomez, C.; Hope, T. J. The ins and outs of HIV replication. *Cell. Microbiol.* **2005**, *7*, 621−626.
(12) Lee, J.-G.; Park, K. R.; An, J. Y.; Kang, J. Y.; Shen, H.; Wang, J.; Eom, S. H. Structural and biochemical insights into inhibition of human primase by citrate. *Biochem. Biophys. Res. Commun.* **2018**, *507*, 383−388.
(13) Zhai, Y.; Sun, F.; Li, X.; Pang, H.; Xu, X.; Bartlam, M.; Rao, Z. Insights into SARS-CoV transcription and replication from the structure of the nsp7-nsp8 hexadecamer. *Nat. Struct. Mol. Biol.* **2005**, *12*, 980−986.
(14) Li, S.; Zhao, Q.; Zhang, Y.; Zhang, Y.; Bartlam, M.; Li, X.; Rao, Z. New nsp8 isoform suggests mechanism for tuning viral RNA synthesis. *Protein Cell* **2010**, *1*, 198−204.
(15) Imbert, I.; Guillemot, J.-C.; Bourhis, J.-M.; Bussetta, C.; Coutard, B.; Egloff, M.-P.; Ferron, F.; Gorbalenya, A. E.; Canard, B. A second, non-canonical RNA-dependent RNA polymerase in SARS coronavirus. *EMBO J.* **2006**, *25*, 4933−4942.
(16) te Velthuis, A. J. W.; van den Worm, S. H. E.; Snijder, E. J. The SARS-coronavirus nsp7+nsp8 complex is a unique multimeric RNA polymerase capable of both de novo initiation and primer extension. *Nucleic Acids Res.* **2012**, *40*, 1737−1747.
(17) Konkolova, E.; Klima, M.; Nencka, R.; Boura, E. Structural analysis of the putative SARS-CoV-2 primase complex. *J. Struct. Biol.* **2020**, *211*, 107548.
(18) Zhang, C.; Li, L.; He, J.; Chen, C.; Su, D. Nonstructural protein 7 and 8 complexes of SARS-CoV-2. *Protein Sci.* **2021**, *30*, 873−881.
(19) Biswal, M.; Diggs, S.; Xu, D.; Khudaverdyan, N.; Lu, J.; Fang, J.; Blaha, G.; Hai, R.; Song, J. Two conserved oligomer interfaces of NSP7 and NSP8 underpin the dynamic assembly of SARS-CoV-2 RdRP. *Nucleic Acids Res.* **2021**, *49*, 5956−5966.
(20) Wilamowski, M.; Hammel, M.; Leite, W.; Zhang, Q.; Kim, Y.; Weiss, K. L.; Jedrzejczak, R.; Rosenberg, D. J.; Fan, Y.; Wower, J.; Bierma, J. C.; Sarker, A. H.; Tsutakawa, S. E.; Pingali, S. V.; O'Neill, H. M.; Joachimiak, A.; Hura, G. L. Transient and stabilized complexes of Nsp7, Nsp8, and Nsp12 in SARS-CoV-2 replication. *Biophys. J.* **2021**, *120*, 3152−3165.
(21) Malone, B.; Chen, J.; Wang, Q.; Llewellyn, E.; Choi, Y. J.; Olinares, P. D. B.; Cao, X.; Hernandez, C.; Eng, E. T.; Chait, B. T.; Shaw, D. E.; Landick, R.; Darst, S. A.; Campbell, E. A. Structural basis for backtracking by the SARS-CoV-2 replication-transcription complex. *Proc. Natl. Acad. Sci. U. S. A.* **2021**, *118*, No. e2102516118.
(22) Wang, Q.; Wu, J.; Wang, H.; Gao, Y.; Liu, Q.; Mu, A.; Ji, W.; Yan, L.; Zhu, Y.; Zhu, C.; Fang, X.; Yang, X.; Huang, Y.; Gao, H.; Liu, F.; Ge, J.; Sun, Q.; Yang, X.; Xu, W.; Liu, Z.; Yang, H.; Lou, Z.; Jiang, B.; Guddat, L. W.; Gong, P.; Rao, Z. Structural basis for RNA replication by the SARS-CoV-2 polymerase. *Cell* **2020**, *182*, 417−428.
(23) Jochheim, F. A.; Tegunov, D.; Hillen, H. S.; Schmitzová, J.; Kokic, G.; Dienemann, C.; Cramer, P. The structure of a dimeric form of SARS-CoV-2 polymerase. *Commun. Biol.* **2021**, *4*, 999.
(24) Hillen, H. S. Structure and function of SARS-CoV-2 polymerase. *Curr. Opin. Virol.* **2021**, *48*, 82−90.
(25) Kokic, G.; Hillen, H. S.; Tegunov, D.; Dienemann, C.; Seitz, F.; Schmitzova, J.; Farnung, L.; Siewert, A.; Höbartner, C.; Cramer, P. Mechanism of SARS-CoV-2 polymerase stalling by remdesivir. *Nat. Commun.* **2021**, *12*, 279.
(26) Yin, W.; Mao, C.; Luan, X.; Shen, D.-D.; Shen, Q.; Su, H.; Wang, X.; Zhou, F.; Zhao, W.; Gao, M.; Chang, S.; Xie, Y.-C.; Tian, G.; Jiang, H.-W.; Tao, S.-C.; Shen, J.; Jiang, Y.; Jiang, H.; Xu, Y.; Zhang, S.; Zhang, Y.; Xu, H. E. Structural basis for inhibition of the RNA-dependent RNA polymerase from SARS-CoV-2 by remdesivir. *Science* **2020**, *368*, 1499−1504.
(27) Yan, R.; Zhang, Y.; Li, Y.; Xia, L.; Guo, Y.; Zhou, Q. Structural basis for the recognition of SARS-CoV-2 by full-length human ACE2. *Science* **2020**, *367*, 1444−1448.
(28) Peng, Q.; Peng, R.; Yuan, B.; Zhao, J.; Wang, M.; Wang, X.; Wang, Q.; Sun, Y.; Fan, Z.; Qi, J.; Gao, G. F.; Shi, Y. Structural and biochemical characterization of the nsp12-nsp7-nsp8 core polymerase complex from SARS-CoV-2. *Cell Rep.* **2020**, *31*, 107774.
(29) Guo, L.; Bi, W.; Wang, X.; Xu, W.; Yan, R.; Zhang, Y.; Zhao, K.; Li, Y.; Zhang, M.; Cai, X.; Jiang, S.; Xie, Y.; Zhou, Q.; Lu, L.; Dang, B. Engineered trimeric ACE2 binds viral spike protein and locks it in "Three-up" conformation to potently inhibit SARS-CoV-2 infection. *Cell Res.* **2021**, *31*, 98−100.
(30) Chen, J.; Malone, B.; Llewellyn, E.; Grasso, M.; Shelton, P. M. M.; Olinares, P. D. B.; Maruthi, K.; Eng, E. T.; Vatandaslar, H.; Chait, B. T.; Kapoor, T. M.; Darst, S. A.; Campbell, E. A. Structural basis for helicase-polymerase coupling in the SARS-CoV-2 replication-transcription complex. *Cell* **2020**, *182*, 1560−1573.
(31) Bravo, J. P. K.; Dangerfield, T. L.; Taylor, D. W.; Johnson, K. A. Remdesivir is a delayed translocation inhibitor of SARS-CoV-2 replication. *Mol. Cell* **2021**, *81*, 1548−1552 e1544.
(32) Kirchdoerfer, R. N.; Ward, A. B. Structure of the SARS-CoV nsp12 polymerase bound to nsp7 and nsp8 co-factors. *Nat. Commun.* **2019**, *10*, 2342.
(33) Naydenova, K.; Muir, K. W.; Wu, L.-F.; Zhang, Z.; Coscia, F.; Peet, M. J.; Castro-Hartmann, P.; Qian, P.; Sader, K.; Dent, K.; Kimanius, D.; Sutherland, J. D.; Lowe, J.; Barford, D.; Russo, C. J. Structure of the SARS-CoV-2 RNA-dependent RNA polymerase in the presence of favipiravir-RTP. *Proc. Natl. Acad. Sci. U. S. A.* **2021**, *118*, No. e2021946118.
(34) Rangan, R.; Zheludev, I. N.; Hagey, R. J.; Pham, E. A.; Wayment-Steele, H. K.; Glenn, J. S.; Das, R. RNA genome conservation and secondary structure in SARS-CoV-2 and SARS-related viruses: a first look. *RNA* **2020**, *26*, 937−959.
(35) Zhang, Y.; Huang, K.; Xie, D.; Lau, J. Y.; Shen, W.; Li, P.; Wang, D.; Zou, Z.; Shi, S.; Ren, H.; Wang, Y.; Mao, Y.; Jin, M.; Kudla, G.; Zhao, Z. In vivo structure and dynamics of the SARS-CoV-2 RNA genome. *Nat. Commun.* **2021**, *12*, 5695.
(36) Cao, C.; Cai, Z.; Xiao, X.; Rao, J.; Chen, J.; Hu, N.; Yang, M.; Xing, X.; Wang, Y.; Li, M.; Zhou, B.; Wang, X.; Wang, J.; Xue, Y. The architecture of the SARS-CoV-2 RNA genome inside virion. *Nat. Commun.* **2021**, *12*, 3917.
(37) Hackbart, M.; Deng, X.; Baker, S. C. Coronavirus endoribonuclease targets viral polyuridine sequences to evade activating host sensors. *Proc. Natl. Acad. Sci. U. S. A.* **2020**, *117*, 8094−8103.
(38) Delano, W. L. *Pymol*; Schrodinger, Inc.. http://pymol.org/.
(39) Schrödinger, LLC.: New York, NY. https://www.schrodinger.com (accessed June 2021).
(40) Cornell, W. D.; Cieplak, P.; Bayly, C. I.; Gould, I. R.; Merz, K. M.; Ferguson, D. M.; Spellmeyer, D. C.; Fox, T.; Caldwell, J. W.; Kollman, P. A. A second generation force field for the simulation of proteins, nucleic acids, and organic molecules (vol 117, pg 5179, 1995). *J. Am. Chem. Soc.* **1996**, *118*, 2309.
(41) Kalé, L.; Skeel, R.; Bhandarkar, M.; Brunner, R.; Gursoy, A.; Krawetz, N.; Phillips, J.; Shinozaki, A.; Varadarajan, K.; Schulten, K. NAMD2: Greater scalability for parallel molecular dynamics. *J. Comput. Phys.* **1999**, *151*, 283−312.
(42) Phillips, J. C.; Braun, R.; Wang, W.; Gumbart, J.; Tajkhorshid, E.; Villa, E.; Chipot, C.; Skeel, R. D.; Kalé, L.; Schulten, K. Scalable molecular dynamics with NAMD. *J. Comput. Chem.* **2005**, *26*, 1781−1802.

https://doi.org/10.1021/acs.biochem.1c00755
Biochemistry XXXX, XXX, XXX−XXX

(43) Humphrey, W.; Dalke, A.; Schulten, K. VMD: visual molecular dynamics. *J. Mol. Graph.* **1996**, *14*, 33−38.
(44) Winn, M. D.; Ballard, C. C.; Cowtan, K. D.; Dodson, E. J.; Emsley, P.; Evans, P. R.; Keegan, R. M.; Krissinel, E. B.; Leslie, A. G. W.; McCoy, A.; McNicholas, S. J.; Murshudov, G. N.; Pannu, N. S.; Potterton, E. A.; Powell, H. R.; Read, R. J.; Vagin, A.; Wilson, K. S. Overview of the CCP4 suite and current developments. *Acta Crystallogr., Sect. D: Biol. Crystallogr.* **2011**, *67*, 235−242.
(45) Murshudov, G. N.; Vagin, A. A.; Dodson, E. J. Refinement of macromolecular structures by the maximum-likelihood method. *Acta Crystallogr., Sect. D: Biol. Crystallogr.* **1997**, *53*, 240−255.
(46) Adams, P. D.; Afonine, P. V.; Bunkóczi, G.; Chen, V. B.; Davis, I. W.; Echols, N.; Headd, J. J.; Hung, L.-W.; Kapral, G. J.; Grosse-Kunstleve, R. W.; McCoy, A. J.; Moriarty, N. W.; Oeffner, R.; Read, R. J.; Richardson, D. C.; Richardson, J. S.; Terwilliger, T. C.; Zwart, P. H. PHENIX: a comprehensive Python-based system for macromolecular structure solution. *Acta Crystallogr., Sect. D: Biol. Crystallogr.* **2010**, *66*, 213−221.
(47) Emsley, P.; Cowtan, K. Coot: model-building tools for molecular graphics. *Acta Crystallogr., Sect. D: Biol. Crystallogr.* **2004**, *60*, 2126−2132.
(48) Kinjo, A. R.; Bekker, G.-J.; Wako, H.; Endo, S.; Tsuchiya, Y.; Sato, H.; Nishi, H.; Kinoshita, K.; Suzuki, H.; Kawabata, T.; Yokochi, M.; Iwata, T.; Kobayashi, N.; Fujiwara, T.; Kurisu, G.; Nakamura, H. New tools and functions in data-out activities at Protein Data Bank Japan (PDBj). *Protein Sci.* **2018**, *27*, 95−102.
(49) Šponer, J.; Bussi, G.; Krepl, M.; Banáš, P.; Bottaro, S.; Cunha, R. A.; Gil-Ley, A.; Pinamonti, G.; Poblete, S.; Jurečka, P.; Walter, N. G.; Otyepka, M. RNA Structural dynamics as captured by molecular simulations: A comprehensive overview. *Chem. Rev.* **2018**, *118*, 4177−4338.
(50) Tan, D.; Piana, S.; Dirks, R. M.; Shaw, D. E. RNA force field with accuracy comparable to state-of-the-art protein force fields. *Proc. Natl. Acad. Sci. U. S. A.* **2018**, *115*, E1346−E1355.
(51) Littler, D. R.; Gully, B. S.; Colson, R. N.; Rossjohn, J. Crystal structure of the SARS-CoV-2 non-structural protein 9, Nsp9. *iScience* **2020**, *23*, 101258.
(52) Zhang, C.; Chen, Y.; Li, L.; Yang, Y.; He, J.; Chen, C.; Su, D. Structural basis of the multimerization of nonstructural protein nsp9 from SARS-CoV-2. *Molecular Biomedicine* **2020**, *1*, 5.
(53) Sutton, G.; Fry, E.; Carter, L.; Sainsbury, S.; Walter, T.; Nettleship, J.; Berrow, N.; Owens, R.; Gilbert, R.; Davidson, A.; Siddell, S.; Poon, L. L. M.; Diprose, J.; Alderton, D.; Walsh, M.; Grimes, J. M.; Stuart, D. I. The nsp9 replicase protein of SARS-coronavirus, structure and functional insights. *Structure* **2004**, *12*, 341−353.
(54) El-Kamand, S.; Du Plessis, M.-D.; Breen, N.; Johnson, L.; Beard, S.; Kwan, A. H.; Richard, D. J.; Cubeddu, L.; Gamsjaeger, R. A distinct ssDNA/RNA binding interface in the Nsp9 protein from SARS-CoV-2. *Proteins* **2022**, *90*, 176−185.
(55) Wang, B.; Svetlov, D.; Artsimovitch, I. NMPylation and de-NMPylation of SARS-CoV-2 nsp9 by the NiRAN domain. *Nucleic Acids Res.* **2021**, *49*, 8822−8835.
(56) Yan, L.; Ge, J.; Zheng, L.; Zhang, Y.; Gao, Y.; Wang, T.; Huang, Y.; Yang, Y.; Gao, S.; Li, M.; Liu, Z.; Wang, H.; Li, Y.; Chen, Y.; Guddat, L. W.; Wang, Q.; Rao, Z.; Lou, Z. Cryo-EM structure of an extended SARS-CoV-2 replication and transcription complex reveals an intermediate state in cap synthesis. *Cell* **2021**, *184*, 184−193.
(57) Slanina, H.; Madhugiri, R.; Bylapudi, G.; Schultheiss, K.; Karl, N.; Gulyaeva, A.; Gorbalenya, A. E.; Linne, U.; Ziebuhr, J. Coronavirus replication-transcription complex: Vital and selective NMPylation of a conserved site in nsp9 by the NiRAN-RdRp subunit. *Proc. Natl. Acad. Sci. U. S. A.* **2021**, *118*, No. e2022310118.

https://doi.org/10.1021/acs.biochem.1c00755
Biochemistry XXXX, XXX, XXX−XXX